

Nonidentical protons

T. Mart and A. Sulaksono

Departemen Fisika, FMIPA, Universitas Indonesia, Depok 16424, Indonesia

(Dated: February 26, 2013)

Abstract

We have calculated the proton charge radius by assuming that the real proton radius is not unique and the radii are randomly distributed in a certain range. This is performed by averaging the elastic electron-proton differential cross section over the form factor cut-off. By using a dipole form factor and fitting the middle value of the cut-off to the low Q^2 Mainz data, we found the lowest χ^2/N for a cut-off $\Lambda = 0.8203 \pm 0.0003$ GeV, which corresponds to a proton charge radius $r_E = 0.8333 \pm 0.0004$ fm. The result is compatible with the recent precision measurement of the Lamb shift in muonic hydrogen as well as recent calculations using more sophisticated techniques. Our result indicates that the relative variation of the form factor cut-off should be around 21.5%. Based on this result we have investigated effects of the nucleon radius variation on the symmetric nuclear matter (SNM) and the neutron star matter (NSM) by considering the excluded volume effect in our calculation. The mass-radius relation of neutron star is found to be sensitive to this variation. The nucleon effective mass in the SNM as well as the equation of state of both the SNM and the NSM exhibit a similar sensitivity.

PACS numbers: 26.60.-c, 21.65.-f, 13.40.Gp, 14.20.Dh

I. INTRODUCTION

The recent precise measurement of the Lamb shift in muonic hydrogen atom [1] has sparked a controversy, because this measurement yields a smaller proton charge radius, i.e. $r_E = 0.84184(67)$ fm. This radius is significantly smaller than the standard CODATA value [2], $r_E = 0.8768(69)$ fm, which is based on the measurements of the Lamb shift in electronic (conventional) hydrogen atom, as well as the results from elastic electron-proton scatterings. The latest precise measurement of elastic electron-proton scattering at MAMI, Mainz, which yields $r_E = 0.879(5)_{\text{stat.}}(4)_{\text{syst.}}(2)_{\text{model}}(4)_{\text{group}}$ fm [3], clearly supports the CODATA value. Considerable efforts [4–21] have been devoted to attack this proton radius problem. References [4, 5], for instance, propose that the off-shell form factors of the proton could generate large polarizability contributions to the proton structure and eventually could solve the problem, since the effect would only appear in the case of muonic Hydrogen. However, a different opinion has been put forward in Ref. [22], in which the off-shell effect is shown to be not sufficiently large to reduce the discrepancy between the radii found in muonic and conventional Hydrogen atoms. It is interesting to note that Ref. [22] also concludes that the resolution of this problem must lie elsewhere, perhaps in re-analyses of the older experiments. Furthermore, QED is believed to be more precise than QCD and the techniques and methods of the Lamb shift measurement in muonic hydrogen as well as electron-proton scattering are beyond any doubts [23]. Therefore, it is urgent to reinvestigate the prevailing methods of extracting the proton charge radius. Such an idea has been recently proposed by a number of research groups [24, 25]. Nevertheless, surprisingly none of them has questioned the idea of the "radius" itself.

The radius of proton is defined in accordance with our imagination that proton has a spherical form. However, recent investigations have revealed that protons could deform from a spherical shape, like nuclei in nuclear physics. This originates from the relativistic motion of the spin 1/2 quarks inside the proton [26], although there is also a claim that a pure s -wave nucleon model, with $l = 0$ and thus perfectly spherical, could be constructed [27]. Meanwhile, in the liquid drop model it is also customary to assume the variation of the proton and neutron radii in order to explain, e.g., the polarized electric dipole moment in the reflection asymmetric nuclei [28]. Obviously, the definition of radius gets blurred if the proton were not spherical.

On the other hand, the fluctuating size of proton has become an important idea in explaining the oscillating color transparency [29]. The idea behind this fluctuating size is that in the proton-nucleus scattering the high energy protons that scattered at wide angles should be "small". However, there is also a certain process, in which the protons must be "large" and the amplitude of this process will increase with increasing the proton sizes. Using this idea the oscillating transparency found in experiment [30], which is defined as the ratio between the proton-proton scattering cross sections off the nucleus and off the proton at 90° as a function of energy, can be successfully reproduced [29].

Based on the above experiences in this paper we propose a calculation of the proton charge radius by assuming that protons do not have identical radii, they vary in a certain range. To simplify the problem we further assume that the radii are randomly distributed around their average value. Practically, since the proton radius enters the cross section via the charge form factor, we can perform this calculation by taking the form factor cut-off as the corresponding variable. We believe that further corrections could enter the cross section formulation. However, for the present exploratory study we also believe that our assumption would be sufficient.

We note that our result is in agreement with that obtained from muonic hydrogen [1]. A more careful measurement has been carried out at Paul Scherer Institute and the result has just been published [32]. It is interesting to note that the latter is still consistent with the previous measurement [1], indicating that the proton radius extracted from muonic hydrogen would hardly change. Therefore, the discrepancy between our result and the electronic hydrogen experiment is still outstanding and more efforts are required to alleviate this problem.

Whereas a five-percent difference in the proton radius could trigger a strong controversy in hadronic studies, it is quite ironic to realize that in the nuclear and neutron star matter investigations protons and neutrons are traditionally considered as "point particles". Effects of the nucleon structures are only considered in the so-called *excluded volume effect* (EVE) model [33–39]. In this model the total volume occupied by N nucleons, i.e. Nv_N , is subtracted from the nuclear matter volume V , so that the effective volume available for the nucleon motion is reduced to $V - Nv_N$, where v_N is the volume of a nucleon. Of course, the volume of the nucleon itself decreases as the matter density increases. However, surprisingly there has been no unique definition of the radius in free space, i.e. at zero-density.

For instance, Ref. [34] used the proton radii $r_p = 0.80$ fm, 0.70 fm, and 0.60 fm to study the EVE on the equation of state of homogeneous hadronic matter, whereas Ref. [33] used $r_p = 0.63$ fm to study the effect on the equation of state of nuclear matter. Nevertheless, all studies indicate that the effect is non-negligible. In fact, Ref. [34] found that the effect can enlarge the range of applicability of the quark-meson-coupling model. Thus, it would be very interesting to study the EVE by using our knowledge obtained from the elastic electron-proton scattering process.

In Sec. II of this paper we explain the procedure of extracting the proton charge form factor. Section III briefly discuss the possible future experiment for refining the present calculation. In Sec. IV we investigate effects of the nucleon radius variation in the neutron star and symmetric nuclear matter. We will summarize and conclude our findings in Sec. V.

II. EXTRACTION OF THE PROTON RADIUS FROM ELECTRON-PROTON SCATTERING

The differential cross section for elastic electron-proton scattering can be efficiently written in terms of the Sachs electric and magnetic form factors, $G_{E,p}$ and $G_{M,p}$, as [40]

$$\frac{d\sigma}{d\Omega} = \left(\frac{d\sigma}{d\Omega} \right)_{\text{Mott}} \frac{1}{(1 + \tau)} \left[G_{E,p}^2(Q^2) + \frac{\tau}{\epsilon} G_{M,p}^2(Q^2) \right], \quad (1)$$

where the Mott cross section,

$$\left(\frac{d\sigma}{d\Omega} \right)_{\text{Mott}} = \frac{E'}{E} \frac{\alpha^2}{4E^2} \frac{\cos^2(\theta/2)}{\sin^4(\theta/2)}, \quad (2)$$

describes the elastic scattering of point-like particle. The notation $\epsilon = [1 + 2(1 + \tau) \tan^2(\theta/2)]^{-1}$ denotes the virtual photon polarization, $Q^2 = 4EE' \sin^2(\theta/2)$ is the square of the virtual photon momentum transfer, $\tau = Q^2/4m_p^2$, m_p is the proton mass, and E (E') represents the electron initial (final) lab energy with scattering angle θ .

Since we will not focus on the problems of extracting the magnetic form factor, we will use the phenomenological scaling $G_{M,p} = \mu_p G_{E,p}$, where μ_p is the proton anomalous magnetic moment, to simplify Eq. (1) to

$$\frac{d\sigma}{d\Omega} = \left(\frac{d\sigma}{d\Omega} \right)_{\text{Mott}} \frac{1}{(1 + \tau)} \left[1 + \frac{\tau}{\epsilon} \mu_p^2 \right] G_{E,p}^2(Q^2, \Lambda), \quad (3)$$

assuming identical charge distributions in the protons, i.e. identical electric and magnetic radii, where Λ is the corresponding cut-off.

However, if the the proton sizes were not identical, and if we assume that they were randomly distributed near their middle value, then Eq. (1) must be averaged over all proton sizes, i.e., averaged over the form factor cut-off Λ ,

$$\left\langle \frac{d\sigma}{d\Omega} \right\rangle = \left(\frac{d\sigma}{d\Omega} \right)_{\text{Mott}} \frac{1}{(1+\tau)} \left[1 + \frac{\tau}{\epsilon} \mu_p^2 \right] \langle G_{E,p}^2(Q^2, \Lambda_1) \rangle, \quad (4)$$

where

$$\langle G_{E,p}^2(Q^2, \Lambda_1) \rangle = \frac{1}{2\Delta\Lambda} \int_{\Lambda_1-\Delta\Lambda}^{\Lambda_1+\Delta\Lambda} G_{E,p}^2(Q^2, \Lambda) d\Lambda, \quad (5)$$

and $2\Delta\Lambda$ represents the range of the cut-off variation around the middle value Λ_1 .

Experimental measurements for decades have indicated that the square root of this average can be parameterized by means of a dipole form,

$$\langle G_{E,p}^2(Q^2, \Lambda_1) \rangle^{1/2} \approx \left(1 + \frac{Q^2}{\Lambda_1^2} \right)^{-2}, \quad (6)$$

where $\Lambda_1^2 = 0.71 \text{ GeV}^2$ is often called as the standard dipole form factor, from which one obtains the proton electric radius by calculating the form factor slope at the real photon point,

$$r_E \equiv \langle r_{E,p}^2 \rangle^{1/2} = \left(-6 \frac{dG_{E,p}(Q^2)}{dQ^2} \Big|_{Q^2=0} \right)^{1/2}. \quad (7)$$

At this stage it is important to note that after the operation of modern continuous beam accelerators, such as MAMI in Mainz and CEBAF at the Jefferson Laboratory, significant deviation from the standard dipole form factor has been observed. To account for this deviation a number of new fits and models has been proposed. This includes modifications of the dipole form [43, 44], as well as introduction of more physical ingredients in the form factor [42, 45]. There seems to be no need to keep the original dipole form to fit both electric and magnetic form factors, especially for a global fit to all data, since the standard dipole is considered as just a phenomenological approximation. Furthermore, the choice of the dipole form also seems to be trivial.

However, in the non-relativistic limit as well as in the Breit frame the dipole form factor is related to an exponentially decaying charge distribution via the Fourier transform. The exponentially decaying behavior is found in most natural phenomena, from radioactive decay rate to atmospheric pressure on earth. Some phenomena in social science also exhibit this

behavior. Thus, we believe that in our present case a dipole form factor looks more natural and a deviation from such a natural phenomenon requires a rigorous physical concept.

Furthermore, it is also important to emphasize here that the determination of the slope at $Q^2 = 0$ given by Eq. (7) requires very good knowledge of $G_{E,p}(Q^2)$ at very low Q^2 . As a consequence, the closer we can approach the real photon point experimentally, the more reliable we can determine the proton charge radius. Therefore, the latest and accurate measurement of the elastic electron-proton scattering with low energy and low Q^2 at MAMI [3] provides very suitable experimental data for our present discussion.

We begin with Eq. (6), which implies that the experimentally observed form factor is in fact an average to the genuine form factor, that one actually should use in Eq. (7) in order to get the real proton radius. As a consequence, the extracted proton radius in this way should be considered as an averaged radius.

To investigate the effect of averaging the form factor given by Eq. (5), let us use the standard dipole form factor to calculate $\langle G_{E,p}^2(Q^2, \Lambda_1) \rangle$ in Eq. (5). Note that if we use a dipole form, the magnitude of the relative variations of both radius r and cut-off Λ are equal, i.e.

$$\left| \frac{\Delta\Lambda}{\Lambda} \right| = \left| \frac{\Delta r}{r} \right|, \quad (8)$$

provided that the variations are not extremely large.

The result is shown in Fig. 1, where we compare our calculations obtained with the cut-off variations $\Delta\Lambda$ from zero up to 40% of its standard value with experimental data. Note that for the sake of simplicity we use the latest result from Mainz experiment [3], which provides the latest and most accurate data in the low Q^2 region, and the result of extraction from the world electron-proton scattering data with two-photon exchange effects included [42], which represents the previous measurements. We use the result obtained from the standard Rosenbluth separation technique for the Mainz data, in order to reduce the model dependency of the data. The $G_{E,p}$ data extracted in Ref. [42] are of course model dependent. However, in this paper they are only used for the purpose of comparison and not included in the fitting database as described in the following discussion.

It is obvious from Fig. 1 that the result shows a variance to the standard dipole form. For $Q^2 \gtrsim 0.25 \text{ GeV}^2$ we observe that the averaged form factors are larger than the standard dipole one (i.e. $\Delta\Lambda/\Lambda = 0$); increasing the relative variation will increase the form factor.

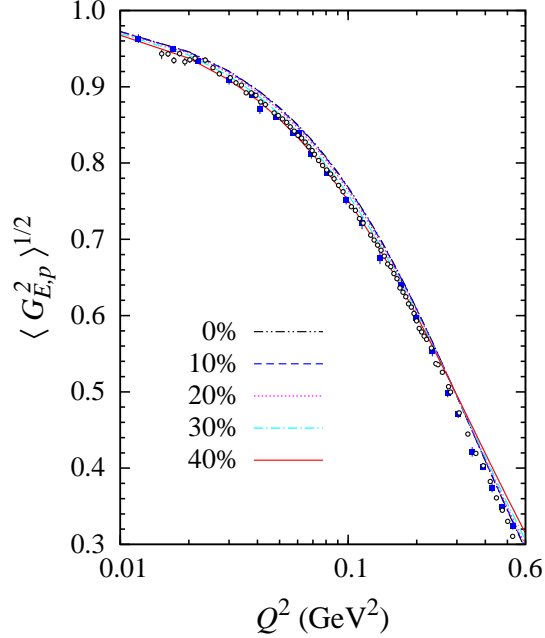


FIG. 1: (Color online) Square root of the averaged $G_{E,p}^2$ calculated from Eq. (5) for different values of the relative variation $\Delta\Lambda/\Lambda_1$ (shown in the figure) compared with experimental data. Experimental data are taken from Refs. [3] (open circles) and [42] (solid squares).

However, for $Q^2 \lesssim 0.25 \text{ GeV}^2$ we observe a different behavior, i.e. the form factor decreases as the variation increases. Since the decrease is relatively small, it is almost invisible in Fig. 1. Therefore, in Fig. 2 we increase the resolution of the $\langle G_{E,p}^2(Q^2, \Lambda_1) \rangle^{1/2}$ axis by limiting $Q^2 \lesssim 0.25 \text{ GeV}^2$, where we can clearly see the effect of variation, i.e. for the relative variation of 40% the agreement with experimental data is almost perfect.

Although the agreement of the solid curve with experimental data in Fig. 2 could be fortuitous, the most important message is that the standard dipole form factor is still valid at low Q^2 , provided that the corresponding cut-off must be averaged with relative variation $\Delta\Lambda/\Lambda_1 = 40\%$. We believe that this is crucial because the extraction of proton charge radius is always plagued with many complicated corrections, especially at high Q^2 regime, as discussed above. In view of this, in what follows, we will only use the MAMI data and limit the Q^2 only up to 0.25 GeV^2 .

It is apparent from Eq. (5) and Fig. 2 that for each value of $\Delta\Lambda$ we can optimize the form factor cut-off Λ_1 in order to further improve the agreement of our calculation with

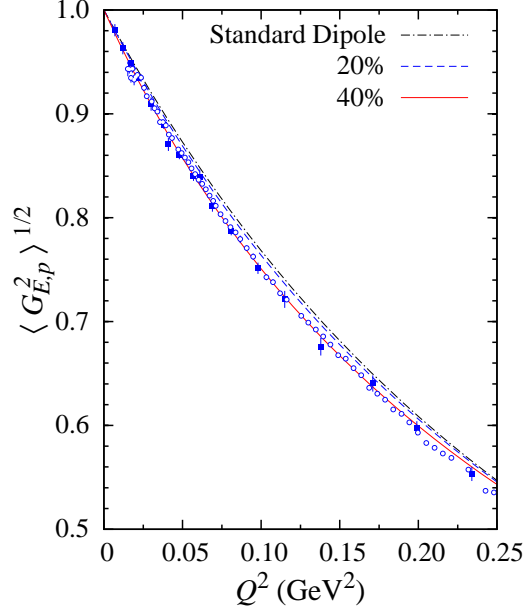


FIG. 2: (Color online) As in Fig. 1, but limited for $Q^2 \leq 0.25$ GeV². The results obtained for two different values of $\Delta\Lambda/\Lambda_1$ are compared with the standard dipole form factor and experimental data. Note the linear scale for Q^2 axis.

experimental data. For this purpose we can calculate the standard χ^2/N which measures the agreement of our calculation with experimental data. The result as functions of the proton radius (translated from Λ_1) and $\Delta\Lambda/\Lambda_1$ is displayed in Fig. 3. It is obvious that the χ^2/N has only one minimum located by the intersection of the two dashed lines.

To locate this minimum accurately we fit the value of Λ_1 by using the CERN-MINUIT code and scan the relative variation $\Delta\Lambda/\Lambda_1$ from 0% to 50% with 2.5% step, simultaneously, where the value of Λ_1 is allowed to vary between 0.80 and 0.90. Although this choice seems to be arbitrary, in our fits we found that the Λ_1 value never reaches both upper and lower limits. For $\Delta\Lambda/\Lambda_1 = 0\%$ (50%) the cut-off value is obtained to be 0.8142 (0.8493) GeV, which corresponds to the proton charge radius of 0.8396 (0.8048) fm.

Having finished the scanning process we observe that the obtained χ^2/N forms a parabola with the minimum value at $\Delta\Lambda/\Lambda_1 = 21.5\%$ and $\Lambda_1 = 0.8203$ GeV. This corresponds to the relative variation of proton radius $\Delta r_E/r_E \approx 21.5\%$, from Eq. (8), and the proton radius of $r = 0.8333$ fm, from Eq. (7). The complete result of this scanning process is depicted in the left panel of Fig. 4. To increase the accuracy, we have refined the $\Delta\Lambda/\Lambda_1$

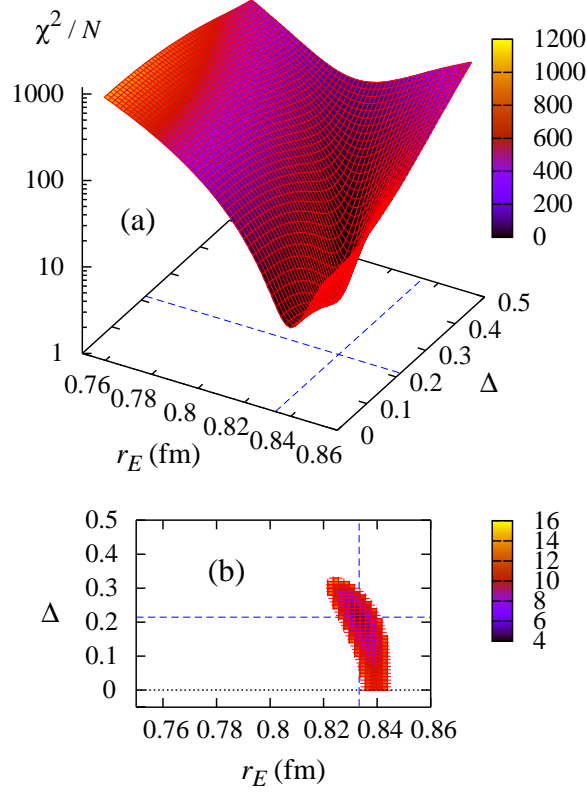


FIG. 3: (Color online) (a) The obtained χ^2/N as functions of the proton charge radius r and $\Delta \equiv \Delta\Lambda/\Lambda_1$. (b) The projection of χ^2/N on the $r - \Delta$ plane for $\chi^2/N \leq 16$. Intersection of the vertical and horizontal dashed lines locates the minimum position of χ^2/N , which is accurately shown in Fig. 4.

step to 0.005, which is equivalent to $\Delta r_E = \pm 0.0003$ fm, in the vicinity of the minimum. Therefore, our calculation would produce the best agreement with experimental data if we used $r_E = 0.8333 \pm 0.0004$ fm, where we have added the error bar coming from the fitting process (Δr obtained from the MINUIT package). The present result is very interesting because it corroborates most of the latest findings that exploits more sophisticated techniques [24, 25].

We have also performed the above procedure to find the proton magnetic radius. It is well known that the experimental data in this case are notoriously inaccurate, especially at $Q^2 \approx 0$. As a consequence, we did not use the four lowest Q^2 data points from Ref. [31], because most of them cannot be renormalized to μ_p at the real photon point. For comparison with the charge radius, we display the result in the right panel of Fig. 4. Obviously, the

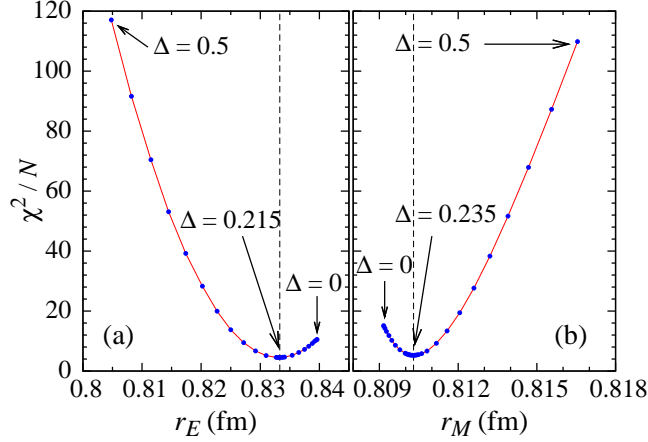


FIG. 4: (Color online) The χ^2/N as a function of the obtained proton (a) charge and (b) magnetic radii. The lowest and highest values of relative variation in the form factor cut-off, $\Delta \equiv \Delta\Lambda/\Lambda_1$, are indicated in the figure. The vertical lines indicate the minimum positions of χ^2/N . The corresponding Δ values are also shown.

trend is different as in the case of the charge radius. In the case of the charge form factor, increasing the relative variation is required to decrease the magnitude of $G_{E,p}$ in order to reproduce experimental data (see Fig. 2). In contrast to this, the relative variation of the radius is required to increase the magnitude of $G_{M,p}$, in order to reproduce the data.

As shown in Fig. 4 we obtain $r_M = 0.8103 \pm 0.0004$ fm, which is smaller than the result extracted from the dispersion relation, i.e. $0.84^{+0.01}_{-0.02}$ fm [24]. Nevertheless, our magnetic radius is much larger than that obtained from direct extraction of the Mainz data, i.e. 0.777 ± 0.013 fm [3]. However, if the Friedrich-Walcher parameterization [43] was used in the latter, the magnetic radius would increase to 0.807 ± 0.02 fm [31], which is apparently in good agreement with our finding. We believe that the less accurate magnetic form factor extracted from the electron-proton scattering could be the origin of the large variance in the extracted magnetic radii found in the literature.

III. EXPECTED FUTURE ELECTRON-PROTON SCATTERING EXPERIMENTS

Since the mathematical formula of the proton charge form factor is in principle not known, determination of the proton radius using Eq. (7) requires very good knowledge of the proton form factor to a very low Q^2 region. Thus, the real challenge for future experiments is to extend the current experimental data to this kinematics. The situation is exhibited in Fig. 5, where we compare the result for the 21.5% proton radius variation obtained in the previous section and various available parameterizations with experimental data [3, 42]. It is obvious from this figure that the Mainz data tend to deviate from our present result, whereas, surprisingly, the data extracted in Ref. [42] show a very good agreement with our calculation. We note that Ref. [42] used polynomial expansion to parameterize the form factor during the extraction. Therefore, we believe that the agreement with the present calculation as exhibited in Fig. 5 could not be a coincidence.

As in the large Q^2 case, in the very low Q^2 region it is also obvious that the standard dipole form factor is substantially larger than our calculation. The result of our calculation is very close to the result obtained from the Friedrich-Walcher model [43]. Since all four models shown in Fig. 5 yield significantly different proton charge radii, it is of course important to refine the experimental measurement at this kinematics. Theoretically, this is possible because Eq. (1) explicitly shows that at low Q^2 contribution of $G_{E,p}$ is dominant. Thus, at low Q^2 measurement of $G_{E,p}$ should be more accurate than that of $G_{M,p}$.

However, from the experimental side this could be a daunting task. It should be remembered that measurements of electron-proton scattering cross section for $Q^2 \approx 0.05 \text{ GeV}^2$ were already at forward angles [31]. Below this point, presumably one has to use other methods. One possible choice proposed at MAMI is the use of the initial state radiation, i.e. radiation emitted by electron before it is scattered by the proton, which could provide measurement of form factors down to $Q^2 = 0.0001 \text{ GeV}^2$ [31]. Obviously, if this method could work, the proton radius would be severely constrained.

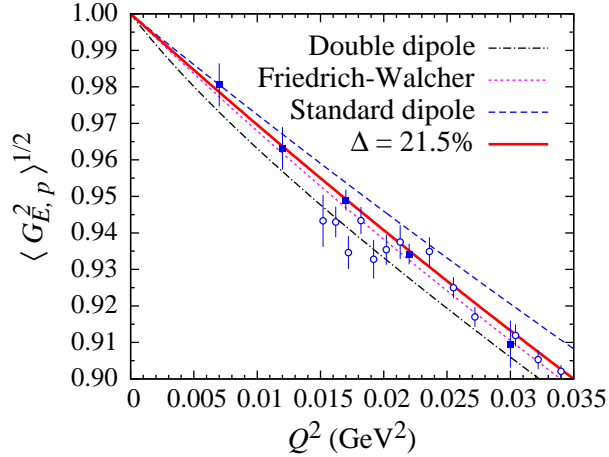


FIG. 5: (Color online) Square root of the averaged $G^2_{E,p}$ obtained from different calculations compared with experimental data for very low Q^2 . Notation for experimental data is as in Fig. 1. Result obtained in the present work is given by the solid curve. Parameters for the double-dipole and Friedrich-Walcher form factors are taken from Ref. [31].

IV. EFFECTS OF THE NUCLEON RADIUS VARIATION ON THE SYMMETRIC NUCLEAR MATTER AND THE NEUTRON STAR MATTER

In the relativistic mean field (RMF) model the Lagrangian density of nucleons consists of four terms, i.e. the free nucleon, free meson, interaction between nucleons via meson exchange, and meson self interaction terms. If we assume that electrons and muons are point particles, whereas nucleons have structures with a radius r_N , then according to the RMF model the energy density of matter consisting of the nucleons and the leptons is given by [39, 41]

$$\begin{aligned} \epsilon = & A(\epsilon_p^k + \epsilon_n^k) + \epsilon_e^k + \epsilon_\mu^k + \epsilon_M(\omega, \sigma, \rho) \\ & + g_\omega \omega_0(\rho_p + \rho_n) + \frac{1}{2} g_\rho b_0(\rho_p - \rho_n), \end{aligned} \quad (9)$$

where g_ω , g_σ and g_ρ are the couplings for ω , σ and ρ mesons, respectively, ϵ_M is the total energy density of the meson, while σ , ω_0 and b_0 are the σ , ω and ρ fields, respectively. Furthermore, in Eq. (9) we have

$$\epsilon_i^k = \frac{2}{(2\pi)^3} \int d^3\vec{k} (k^2 + m_i^{*2})^{1/2} \theta(k - k_F), \quad i = p, n, e, \mu, \quad (10)$$

where for leptons the effective mass is $m_i^* = m_i$ and for nucleons $m_i^* = m_i - g_\sigma \sigma$.

The nucleon and scalar densities read

$$\rho_i = A \bar{\rho}_i, \quad (11)$$

$$\rho_{s,i} = A \bar{\rho}_{s,i}, \quad (12)$$

where $\bar{\rho}_i$ and $\bar{\rho}_{s,i}$ are the i th nucleon and scalar densities, assuming the nucleon is a point particle. The normalization constant A is given by

$$A = \frac{1}{1 + V_p \bar{\rho}_p + V_n \bar{\rho}_n}, \quad (13)$$

with V_p and V_n the proton and neutron volumes, respectively. To simplify the present calculation we assume that

$$V_p = V_n \equiv V_N = \frac{4}{3} \pi r_N^3, \quad (14)$$

where V_N and r_N are the volume and radius of the nucleon, respectively.

From Eq. (9) we can derive the matter pressure,

$$P = \rho^2 \frac{d\varepsilon}{d\rho}, \quad (15)$$

with $\varepsilon = \epsilon/\rho$. Furthermore, the chemical potential for the i th nucleon can be obtained from

$$\mu_i = E_{F,i}^* + V_i P_i' + g_\omega \omega_0 + \alpha_i \frac{1}{2} g_\rho b_0, \quad (16)$$

with α_i equals $+1$ (-1) for proton (neutron), $E_{F,i}^* = (k_{F,i}^2 + m_i^{*2})^{1/2}$ and

$$\begin{aligned} P_i' = & \frac{1}{12\pi^2} \left\{ E_{F,i}^* k_{F,i} \left(E_{F,i}^{*2} - \frac{5}{2} m_i^{*2} \right) \right. \\ & \left. + \frac{3}{2} m_i^{*4} \log \left(\frac{k_{F,i} + E_{F,i}^*}{m_i^*} \right) \right\}. \end{aligned} \quad (17)$$

Different from the quark meson coupling (QMC) model [34, 36], where the dependence of r_N on the matter density can be directly obtained from the model, in the RMF approach the dependence cannot be easily predicted. Therefore, in the present study we choose a phenomenological form for the nucleon radius, which is given by

$$r_N(\rho) = r_N(0) \left\{ 1 + \beta \left(\frac{\rho}{\rho_0} \right)^2 \right\}^{-2}, \quad (18)$$

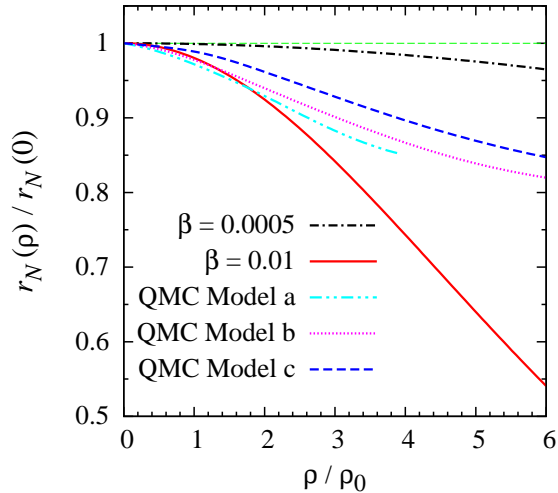


FIG. 6: (Color online) Comparison between proton bag radii as a function of the ratio between nucleon and nuclear saturation densities obtained from the QMC models [34] and Eq. (18) with two different β values.

where $\rho = \rho_p + \rho_n$, ρ_0 is the value of ρ at saturation point, and $r_N(0)$ is the proton radius in vacuum (zero density), determined from Eq. (7). At first glance, the choice seems to be trivial. However, it is actually selected to fulfill the causality constraint. Furthermore, the formula given in Eq. (18) is more convenient for the present purpose, rather than the exponential one, because in the framework of the presently used RMF model we found that the required radius must slowly fall off as a function of density. Otherwise, the predicted neutron star mass would violently overshoot the mass of the SRJ164-2230 pulsar, which is believed to be the heaviest observed neutron star [46]. We also observed that, for selected value of β , Eq. (18) can be adjusted to mimic the result of the QMC models [34] in a certain range of density, thus providing a good check of our result.

The ratio between $r_N(\rho)$ and $r_N(0)$ is exhibited in Fig. 6, where we compare the results obtained from two β values, i.e. $\beta = 0.0005$ and 0.01 , with those obtained from the QMC calculation using different values of bag constants B (see Ref. [34] for explanation). It is apparent from this figure that the difference between the calculated radii increases as the density increases. Nevertheless, the distributions of the radii obtained from the QMC model are still bounded within the difference of the two chosen β values in Eq. (18), i.e. the solid and dash-dotted lines in Fig. 6.

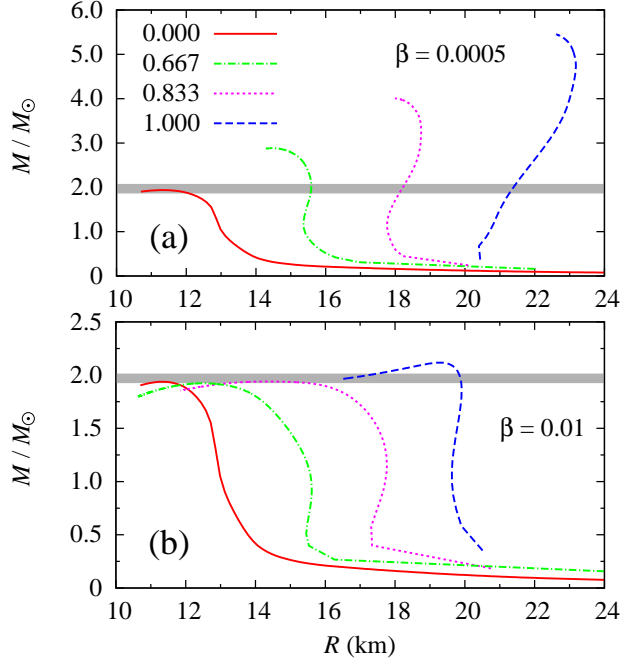


FIG. 7: (Color online) The neutron star mass as a function of its radius for four different nucleon radius assumptions. Panels (a) and (b) show the calculation with $\beta = 0.0005$ and $\beta = 0.01$ in Eq. (18), respectively. The gray horizontal bands show the mass of the SRJ164-2230 pulsar, which is believed to be the heaviest observed neutron star [46]. Notation of the curves in both panels is given in Fig. 8.

For the RMF model we use the parameter set obtained by the IUFSU collaboration [47]. In calculating the equation of state (EOS) of the neutron star matter (NSM) we use the neutrality and β -stability conditions. They are required in calculating the Fermi momentum of each particle in the neutron star core.

The neutron star mass as a function of its radius can be obtained by solving the Tolman-Oppenheimer-Volkoff (TOV) equation with different particle densities in the neutron star core. In order to describe the "outer crust" region we have used the EOS given by R  ster *et al.* [48]. The EOS for the "inner crust" region is obtained from an extrapolation of the EOS of the core and "outer crust" by making use of the polytropic energy-pressure density approximation. The "crust" region is described by using the RMF model with and without the EVE.

Since in the nuclear and neutron star matter a direct comparison between model calcu-

lations and precise experimental data, as in the case of electron-proton scattering in the previous section, is beyond our imagination at present, in the followings we will not calculate the effect of averaging the nucleon radius on the possible observables. Furthermore, as already obtained in the previous section, the effect of this averaging process is a relatively tiny shift from the original value. Therefore, we believe that at this stage it is sufficient to investigate the effect on the conventional observables by using a $\pm 20\%$ variation of the nucleon original radius. Note that this variation enters our calculation through Eqs. (13) and (14).

Figure 7 shows the sensitivity of the neutron star mass-radius relation to the variation of the nucleon radius as well as to the dependence of the nucleon radius on the matter density [β in Eq. (18)], in the framework of RMF models. The radius of the neutron star depends on the value of nucleon radius, whereas the maximum mass of the neutron star is controlled by the dependence of the nucleon radius on the matter density. Therefore, the heaviest observed neutron star mass PSRJ1614-2230 [46] shown by the horizontal gray lines in Fig. 7 yields a significant suppression of the nucleon radius at very high density. This result is interesting, because it opens the possibility of hyperon existence in a neutron star by using the hyperon vector couplings obtained from SU(6) symmetry [49].

With regard to the radius of the canonical neutron star ($1.4M_\odot$), which is constrained between 10.4 km and 12.9 km [50], our present result should be carefully interpreted, because in this calculation we have used the IUFSU parameter set, which was fitted to the finite nuclei data by assuming point particle approximation for the nucleon. Therefore, the present result cannot be quantitatively compared with those obtained with other constraints. Nevertheless, Fig. 7 indicates that the present result could become a stringent constraint to the nucleon radius at high density, once a consistent EOS with EVE were available.

Since the result obtained by using $\beta = 0.0005$ substantially overshoots the PSRJ1614-2230 constraint, as shown in Fig. 7, in the following discussion we will only use $\beta = 0.01$. The result for the effective nucleon mass in the case of symmetric nuclear matter (SNM) is shown in Fig. 8, where we compare the calculated masses obtained by assuming point particle approximation [$r_N(0) = 0$] and finite nucleon radii [$r_N(0) \neq 0$].

From Fig. 8 it is apparent that at high densities the nucleon effective mass increases with increasing the nucleon radius. In view of the instability against the particle-hole excitation at high densities due to the density fluctuation [51], a sufficiently large effective mass predicted

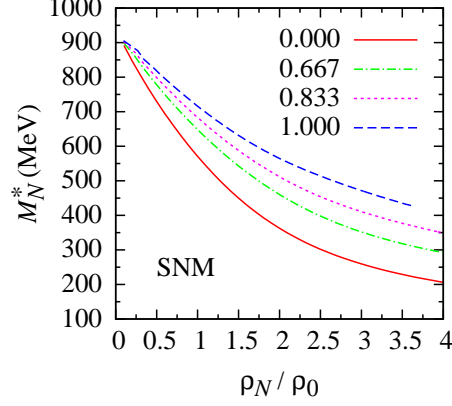


FIG. 8: (Color online) Effective nucleon mass as a function of the ratio between nucleon and nuclear saturation densities. The results are obtained with different values of the nucleon radius $r_N(0)$ as indicated in the figure (in the unit of fm).

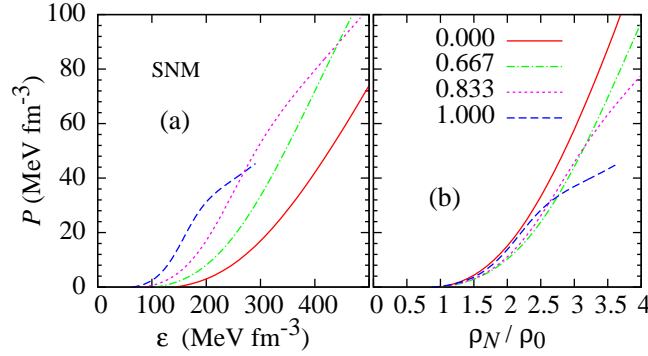


FIG. 9: (Color online) Equation of states of the symmetric nuclear matter obtained from calculations with different values of the nucleon radius as a function of (a) energy and (b) density. Notation of the curves is as in Fig. 8.

by the RMF model has an obvious advantage.

Figures 9 and 10 exhibit the non-zero nucleon radius effect on the EOS of SNM and NSM, respectively. The solid circles in the NSM EOS of Fig. 10 indicate the positions of the NS center pressures and center energy densities of maximum mass. At moderate densities, which correspond to $\epsilon \lesssim 300$, we observe that the EOS becomes stiffer as the nucleon radius increases. Beyond this range, the EOS tends to be softer. From Fig. 11, it is obvious that the pressure of the NS center with maximum mass of $r_N(0) = 1$ fm (blue dashed line) is

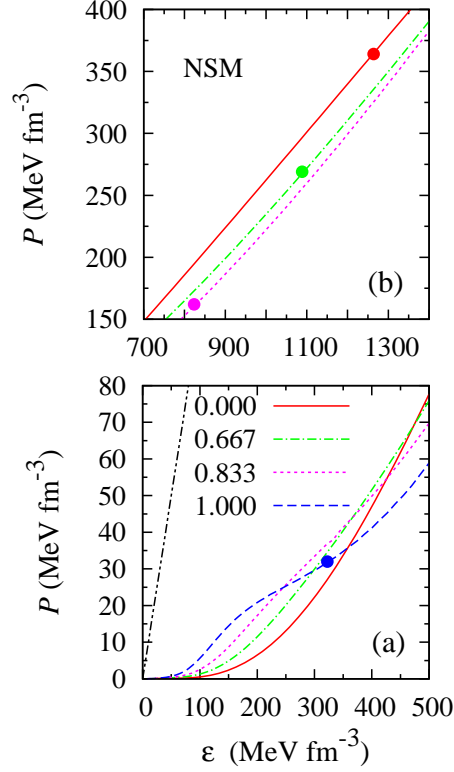


FIG. 10: (Color online) As in Fig. 9a, but for the neutron star matter at (a) lower and (b) higher energies. The dash-dot-dotted line in panel (a) shows the causality constraint, the solid circles indicate the center pressures and energy densities in the neutron star with maximum mass.

approximately 32 MeV fm^{-3} , which corresponds to the energy density of about 320 MeV fm^{-3} . At this point the EOS obtained with $r_N(0) = 1 \text{ fm}$ is stiffest compared to other cases [panel (a) of Fig. 10]. Since in obtaining the NS mass we should integrate the TOV equation using the corresponding EOS as input from the NS center pressure up to zero, information based solely on the soft EOS at high densities of $r_N(0) = 1 \text{ fm}$ is insufficient for a complete understanding of the NS maximum mass. For other non zero nucleon radius cases, the situation is similar.

Obviously, decreasing the nucleon radius will decrease the pressure in the region of $\epsilon \leq 300 \text{ MeV fm}^{-3}$. However, decreasing the nucleon radius will simultaneously increase the NS center pressure. Thus, additional contribution from the center pressure up to 300 MeV fm^{-3} will only slightly increase the NS mass. This is due to the fact that the corresponding EOS at high densities are relatively soft. On the other hand, in the case of zero nucleon radius

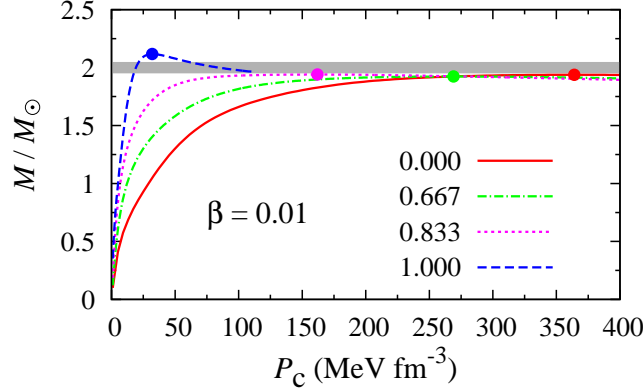


FIG. 11: (Color online) Neutron star mass as a function of its center pressure for different nucleon radii obtained with $\beta = 0.01$. Solid circles indicate the maximum masses with the corresponding center pressures.

but using the same RMF parameter set, the contribution from 300 MeV fm^{-3} up to zero is very small but the contribution from high densities is dominant because the corresponding EOS is stiffer than that of the nonzero nucleon radius. The very small contribution in the region $\leq 300 \text{ MeV fm}^{-3}$ and the relatively large center pressure are typical for point-particle RMF models. In this case, the strong correlation between the NS maximum mass and the EOS stiffness at high densities is very obvious. Therefore, in the point particle case we only need to consider the EOS at high densities in investigating the NS maximum mass behavior. In addition, the high densities EOS become significantly stiffer as β decreases, As a consequence, decreasing the β value will increase the maximum mass of NS. Thus, the increasing of the NS mass depends sensitively on the nucleon radius in free space. These phenomena explain the increase of the predicted mass and radius of the neutron star with increasing the nucleon radius, as shown in Fig. 7.

In Fig. 12 we display the finite nucleon radius effect on the fraction of the matter constituents in the neutron star. It is obvious from this figure that increasing the nucleon radius will increase the number of existing charge particles at high density. This result has a serious consequence on a number of neutron star properties, such as the neutron star stability, neutrino transport in the neutron star, as well as the cooling process of a neutron star. Unfortunately, a more detailed and quantitative analysis of the EVE on neutron star should wait for a more consistent EOS, which includes the EVE in the calculation.

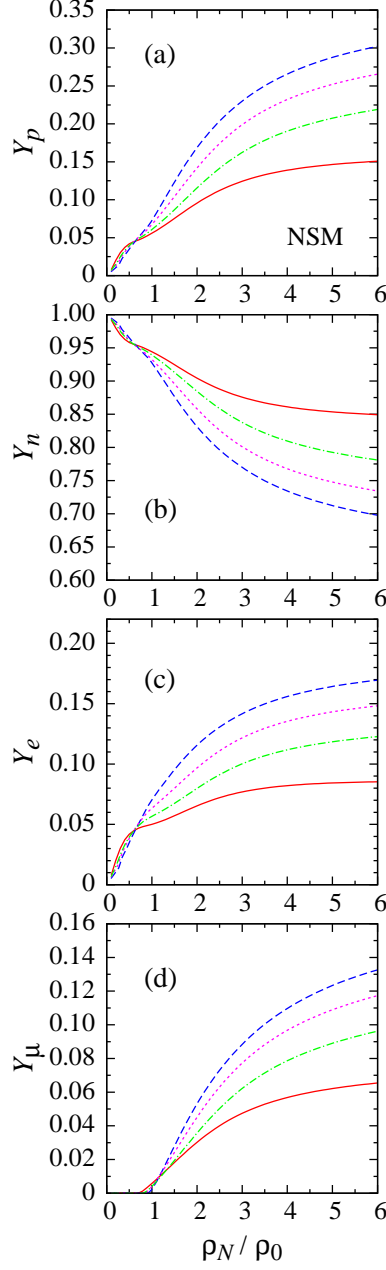


FIG. 12: (Color online) Proton, neutron, electron, and muon fractions in the neutron star matter as a function of the ratio between nucleon and nuclear saturation densities. Notation of the curves is as in Fig. 8.

V. SUMMARY AND CONCLUSION

We have investigated effects of the proton radius variation on the extraction of the proton charge form factor. To achieve the best agreement with experimental data we have averaged

a dipole form factor over the corresponding cut-off with an upper (lower) integration limit of +21.5% (−21.5%) from its middle value. The extracted proton charge radius is found to be smaller than that obtained using the traditional standard dipole fit, but is in good agreement with those obtained from a recent measurement of the Lamb shift in muonic hydrogen atom as well as from the dispersion relation. The extracted proton magnetic radius is smaller than the result of the dispersion relation, but in agreement with the direct extraction by making use of the Friedrich-Walcher form factor. Nevertheless, since the magnetic form factor is less accurate, the extraction of magnetic radius is also less reliable as compared to the result of the charge radius.

We have also investigated effects of the nucleon radius variation on the SNM and the NSM. To this end, the nucleon radius dependence on the matter density is described by a simple phenomenological form and four assumptions of the nucleon radius at zero density are considered in the calculation, i.e. 0 fm (point particle approximation), 0.833 fm (original radius), as well as 0.667 fm and 1.000 fm ($\pm 20\%$ modifications of the original radius). We found that the relation between the mass and radius of a neutron star is very sensitive to the radius of the nucleon. A similar result is also observed in the case of the effective nucleon mass of the SNM as well as the EOS of both NSM and SNM. However, a more quantitative conclusion could be drawn only after a more consistent EOS, with the EVE considered, had been available.

Acknowledgment

This work has been supported in part by the University of Indonesia and the Competence Grant of the Indonesian Ministry of Education and Culture.

-
- [1] R. Pohl, *et al.*, Nature **466**, 213 (2010).
 - [2] P. J. Mohr, B. N. Taylor and D. B. Newell, Rev. Mod. Phys. **80**, 633 (2008).
 - [3] J. C. Bernauer *et al.* [A1 Collaboration], Phys. Rev. Lett. **105**, 242001 (2010).
 - [4] G. A. Miller, A. W. Thomas, J. D. Carroll, J. Rafelski, Phys. Rev. A **84**, 020101 (2011).
 - [5] G. A. Miller, A. W. Thomas, J. D. Carroll, arXiv:1207.0549 [nucl-th].
 - [6] J. Jaeckel and S. Roy, Phys. Rev. D **82**, 125020 (2010).

- [7] A. De Rujula, Phys. Lett. B **693**, 555 (2010).
- [8] I. C. Cloet and G. A. Miller, Phys. Rev. C **83**, 012201 (2011).
- [9] D. Tucker-Smith and I. Yavin, Phys. Rev. D **83**, 101702 (2011).
- [10] B. Batell, D. McKeen, and M. Pospelov, Phys. Rev. Lett. **107**, 011803 (2011).
- [11] R. J. Hill and G. Paz, Phys. Rev. Lett. **107**, 160402 (2011).
- [12] V. Barger, C.-W. Chiang, W.-Y. Keung and D. Marfatia, Phys. Rev. Lett. **106**, 153001 (2011).
- [13] J. D. Carroll, A. W. Thomas, J. Rafelski, and G. A. Miller, Phys. Rev. A **84**, 012506 (2011).
- [14] U. D. Jentschura, Annals Phys. **326**, 500 (2011); *ibid.*, 516 (2011).
- [15] P. Brax and C. Burrage, Phys. Rev. D **83**, 035020 (2011).
- [16] J. I. Rivas, A. Camacho and E. Göklü, Phys. Rev. D **84**, 055024 (2011).
- [17] A. Pineda, Talk given at 14th International Conference on Hadron Spectroscopy (Hadron 2011) [arXiv:1108.1263 [hep-ph]].
- [18] C. E. Carlson, V. Nazaryan and K. Griffioen, Phys. Rev. A **83**, 042509 (2011).
- [19] V. Barger, C. -W. Chiang, W. -Y. Keung and D. Marfatia, Phys. Rev. Lett. **108**, 081802 (2012).
- [20] E. Borie, Annals Phys. **327**, 733 (2012).
- [21] M. I. Eides, Phys. Rev. A **85**, 034503 (2012) [arXiv:1201.2979 [physics.atom-ph]].
- [22] M. C. Birse and J. A. McGovern Eur. Phys. J. A **48**, 120 (2012).
- [23] M. O. Distler, J. C. Bernauer and T. Walcher, Phys. Lett. B **696**, 343 (2011) [arXiv:1011.1861 [nucl-th]].
- [24] I. T. Lorenz, H. -W. Hammer and U. -G. Meissner, Eur. Phys. J. A **48**, 151 (2012) [arXiv:1205.6628 [hep-ph]].
- [25] N. G. Kelkar, F. G. Daza and M. Nowakowski, Nucl. Phys. B **864**, 382 (2012) [arXiv:1203.0581 [hep-ph]].
- [26] A. Kvinikhidze and G. A. Miller, Phys. Rev. C **73**, 065203 (2006); Phys. Rev. C **76**, 025203 (2007).
- [27] F. Gross and P. Agbakpe, Phys. Rev. C **73**, 015203 (2006)
- [28] V. Yu. Denisov, Eur. Phys. J. A **47**, 80 (2011).
- [29] J. P. Ralston and B. Pire, Phys. Rev. Lett. **61**, 1823 (1988).
- [30] A. S. Carroll *et al.*, Phys. Rev. Lett. **61**, 1698 (1988).
- [31] J. C. Bernauer, Ph.D. Thesis, Universität Mainz, 2010.

- [32] A. Antognini *et al.*, Science **339**, 417 (2013).
- [33] Bao-Xi Sun, Xiao-Fu Lu, and En-Guang Zhao, Phys. Rev. C **65**, 054301 (2002).
- [34] R. M. Aguirre and A. L. De Paoli, Phys. Rev. C **68**, 055804 (2003).
- [35] R. M. Aguirre and A. L. De Paoli, Phys. Rev. C **75**, 045207 (2007).
- [36] P. K. Panda, M. E. Bracco, M. Chiapparini, E. Conte, and G. Krein, Phys. Rev. C **65**, 065206 (2002).
- [37] B. K. Patra and C. P. Singh, Nucl. Phys. A **614**, 337 (1997).
- [38] D. V. Anghel, A. S. Parvan, A. S. Khvorostukhin, Physica A **391**, 2313 (2012).
- [39] H. Kouno, K. Koide, T. Mitsumori, N. Noda, A. Hasegawa, Prog. Theor. Phys. **96**, 191 (1996).
- [40] F. Halzen and A. D. Martin, *Quarks and Leptons: An Introductory Course in Modern Particle Physics* (John Wiley & Sons, New York), p. 175.
- [41] D. H. Rischke, M. I. Gorenstein, H. Stöcker and W. Greiner, Z. Phys. C **51**, 485 (1991).
- [42] J. Arrington, W. Melnitchouk, and J. A. Tjon, Phys. Rev. C **76**, 035205 (2007).
- [43] J. Friedrich and Th. Walcher, Eur. Phys. J. A **17**, 607 (2003).
- [44] J. Arrington, Phys. Rev. C **69**, 022201 (2004).
- [45] E. L. Lomon, Phys. Rev. C **64**, 035204 (2001).
- [46] P. B. Demorest, T. Pennuci, S. M. Ransom, M. S. E. Roberts and J. W. T. Hessels, Nature **467**, 1081 (2010).
- [47] F. J. Fattoyev, C. J. Horowitz, J. Piekarewicz, and G. Shen, Phys. Rev. C **82**, 055803 (2010).
- [48] S. B. Rüster, M. Hempel and J. Schaffner-Bielich, Phys. Rev. C **73**, 035804 (2006).
- [49] S. Weissenborn, D. Chatterjee and J. Schaffner-Bielich, Phys. Rev. C **85**, 065802 (2012).
- [50] A. W. Steiner, J. M. Lattimer , and E. F. Brown, arXiv:1205.6871 (2012).
- [51] A. Sulaksono , T. J. Bürvenich , P.-G. Reinhard , and J. A. Maruhn, Phys. Rev. C **79**, 044306 (2009).